LASER PYROLYSIS SYNTHESIZED IRON OXIDE NANOPARTICLES. A STUDY ON THE INFLUENCE OF THE SENSITIZER USED

Iulia Ioana LUNGU[1], Ecaterina ANDRONESCU[2,3]*, Florian DUMITRACHE[1], Lavinia GAVRILA-FLORESCU[1], Iuliana MORJAN[1], Ana Maria BANICI[1], Claudiu FLEACA[1], Anca CRIVEANU[1], Gabriel PRODAN[4]

The synthesis of iron oxide nanoparticles by laser pyrolysis has gained significant attention due to its several advantages over classical methods, including control over experimental parameters, and narrow size distribution. The novelty of this study comes from the comparison between two different sensitizers used in the synthesis process and the influence on the resulted nanoparticles.

The morpho-structural characterization of the nanoparticles has been attained using XRD and TEM, confirming the magnetite/maghemite phase, as well as their nanometric sizes. Their stability was confirmed by DLS analysis and further insight into the C content determined by the sensitizers was analysed using XPS.

Keywords: laser pyrolysis, sensitizer, nanoparticles

1. Introduction

It is already known that the unique properties of iron oxide nanoparticles are what lead them to be intensely researched for various applications. In order to attain said features, a critical factor is choosing the appropriate synthesis method [1, 2]. In this regard, laser pyrolysis is a versatile and efficient technique that can be used to obtain tailor-made iron oxide nanoparticles [3-8]. For obtaining these nanoparticles, iron pentacarbonyl ($Fe(CO)_5$) is the main precursor used, in the form of vapours [9-11].

The main principle of laser pyrolysis is the resonance between the emission line of the laser and the absorption line of the gas precursor. However, if the gas mixture containing the precursor does not have an absorption band at the needed wavelength, a sensitizer is used in order to transfer the energy through collision [12]. As an example, one of the most common sensitizers used is ethylene (C_2H_4) which has a significant absorption due to the fundamental frequencies (949.3 cm^{-1} and 940.6 cm^{-1}) that are close to the frequency of the CO_2 laser radiation

[1] National Institute for Laser, Plasma and Radiation Physics, Magurele Platform, Romania
[2] Faculty of Applied Chemistry and Materials Science, The National University of Science and Technology POLITEHNICA Bucharest, Romania
[3] * Academy of Romanian Scientists, Bucharest, Romania, correspondence author, e-mail: ecaterina.andronescu@upb.ro
[4] "Ovidius" University of Constanta, Romania

(944 cm^{-1}). Another example, however, with a weaker absorption at the required wavelength, is isopropanol (C_3H_8O) [13, 14].

One of the advantages of using a lower absorption sensitizer is that the energy transfer generated due to the laser-molecule interaction is not a high. The molecular excitation process on the resonant level, as well as the thermalisation process following intermolecular collisions, are obtained without heavily affecting the decomposition of the sensitizer agent. As a result, the carbon content of the attained iron oxide nanoparticles is lower than in the case of a high absorption sensitizer.

Herein, we present the synthesis of iron oxide nanoparticles by laser pyrolysis using two sensitizer (high and low absorption) and the subsequent characterization and C content evaluation of these nanoparticles.

2. Experimental

a. Materials and methods

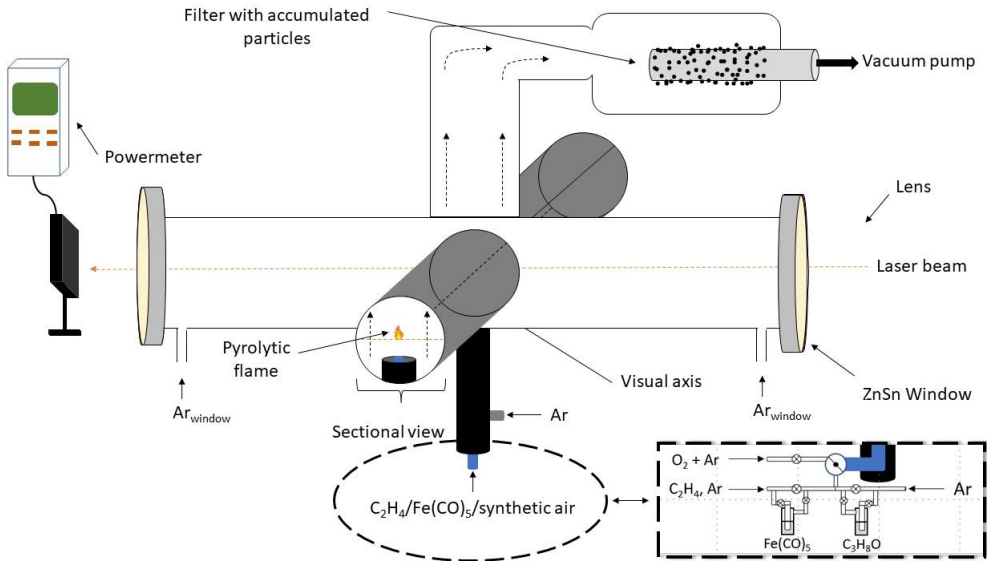

Fig. 1. Laser pyrolysis experimental set-up for iron oxide nanoparticle synthesis using ethylene/isopropanol as sensitizer

Iron oxide nanoparticles were synthesized by laser pyrolysis using the experimental installation presented in Fig. 1. The highlighted parts represent the small alteration attained for different sensitizers (circle, centre – ethylene, square, right – isopropanol).Briefly, the method is based on the cross-flow configuration of the reaction chamber that permits the interaction between the emission line of the CO_2 IR laser and the absorption line of the sensitizer, which subsequently heats the reactive mixture through collision energy transfer [1].

A CO_2 laser in a cvasi-continuum regime was used at an operating $\lambda = 10.59$ μm. The iron precursor was $Fe(CO)_5$ and the sensitizers were C_2H_4 and C_3H_8O. A coaxial Ar flow has a double role of ensuring the confinement of the gas precursors towards the flow axis and maintaining the freshly nucleated particles towards the collection chamber. The process was described in detail elsewhere [1].

The following hypothesis is used: the quantity of the volatile precursor is based on the ratio between its saturated vapours pressure and the pressure difference until the one from the reaction chamber. For example, for an Ar flow of 66 sccm that enters the $Fe(CO)_5$ containing bubbler ($Fe(CO)_5$ in liquid form), at an ambient temperature of 25°C, the estimated flow will be 9.57 sccm determined by the bubbler formula [15]. Iron pentacarbonyl pressure vapours were determined by Antoine Equation using the parameters provided by webbook.nist.gov. The same method can be used to calculate the flow of isopropanol vapours. The experimental parameters for both samples are presented in Table 1.

Table 1

Experimental parameters

Sample	Gas Flow Rates	Pressure and Power	Other parameters
e-FeO_x	$D_{C2H4/Fe(CO)5}$ = 33/4.78 sccm D_{air} = 33 sccm	P_{Lar} = 80 W P_{Lab} = 75 W p = 300 mbar	T_{fl} = 485 °C d_{fl} = 28 cm φ_{fl} = 0.2 cm
i-FeO_x	$D_{Ar/Fe(CO)5}$ = 66/9.57 sccm $D_{Ar/C3H8O}$ = 66/11.34 sccm D_{O2} = 26 sccm	P_{Lar} = 305 W P_{Lab} = 300 W p = 300 mbar	T_{fl} = 505 °C d_{fl} = 26.5 cm φ_{fl} = 0.15 cm

After synthesis, the samples were characterized using dynamic light scattering (DLS) in regard to their hydrodynamic dimensions, polydispersity index and zeta potential using a Nanoparticle Analyzer SZ-100V2, Horiba apparatus. In order to attain this characterization, suspensions of the samples were obtained by adding the corresponding quantity of 0.5 g/L sample in 50 mL distilled water. The suspensions were then treated in an ultrasound bath at 59 kHz for 30 min at 20°C (temperature maintained using a coiled cooling system). The pH of the samples and a blank of distilled water was also measured, and both samples displayed pH of around 5, while the blank has a pH of almost 6. The samples were measured in triplicate and the results are presented in Table 2.

The samples were also characterized regarding their crystallinity which was evaluated using a PANalytical X'Pert3 Powder X-ray diffractometer (XRD). The apparatus used a Cu Kα radiation source (wavelength of 1.5418 Å).

Table 2

DLS measurements

Sample	Z-average	PDI	Zeta potential
	nm		mV
e-FeO_x	181.5	0.465	61.43
i-FeO_x	95.9	0.373	49.3

A side-by-side comparison between the two samples is presented in Fig. 2. The mean crystallite dimension was calculated using Debye-Sherrer Equation based on the position and half-length width of the peak (440).

Morpho-structural characterization of the samples was attained by transmission electron microscopy (TEM) and selected area electron diffraction (SAED) using a Philips CM 120ST (120kV) apparatus.

Elemental analysis of the obtained powders was obtained using energy-dispersive X-ray spectroscopy (EDS) using a FEI Quanta Inspect S scanning electron microscope (SEM) operating at 10 kV accelerating voltage and equipped with a EDAX apparatus and X-ray photoelectron spectroscopy (XPS) using a ESCALAB Xi^+ (Thermo Scientific Surface Analysis) facility. The elemental composition evaluated by both techniques can be observed in Table 3, whereas the spectra for both samples can be seen in Fig. 2. Fig. 5 and 6 represent the spectra for high-resolution O 1s and C 1s for both FeO_x samples.

Table 3

Elemental composition evaluated by EDS and XPS analysis

Sample / Element	C (at.%)	O (at.%)	Fe (at.%)
EDS			
e-FeO_x	1.73	61.37	36.90
i-FeO_x	1.47	61.04	37.49
XPS			
e-FeO_x	30.14	50.19	19.67
i-FeO_x	18.87	53.38	27.75

The active zone for the lighter elements C $_K$, O $_K$, and Fe $_L$ that can be identified are presented in Fig. 2.

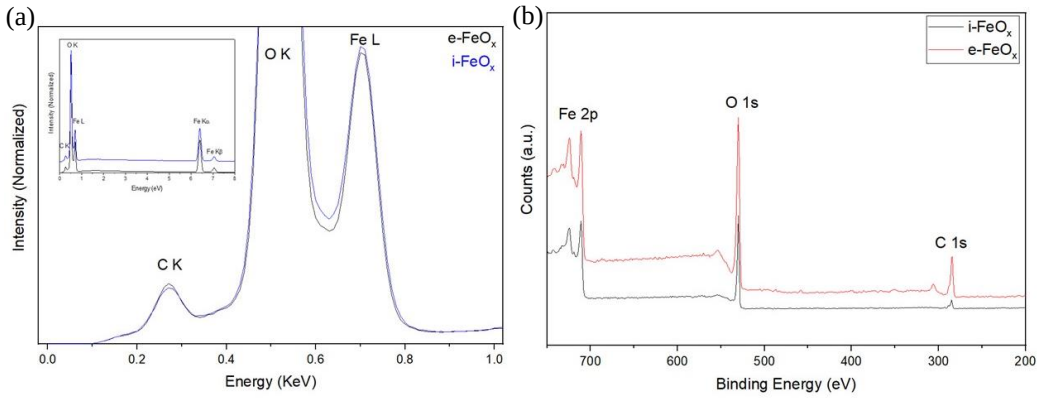

Fig. 2. (a) EDS spectra and (b) XPS spectrum of survey scan for the analysed samples

b. Results and discussions

Two experiments have been successfully conducted for obtaining iron oxide nanoparticles, one with ethene as sensitizer, and one with isopropanol. Both samples have been investigated and characterized from a morpho-structural point of view using TEM and XRD. Fig. 3 shows the diffraction pattern of the investigated samples.

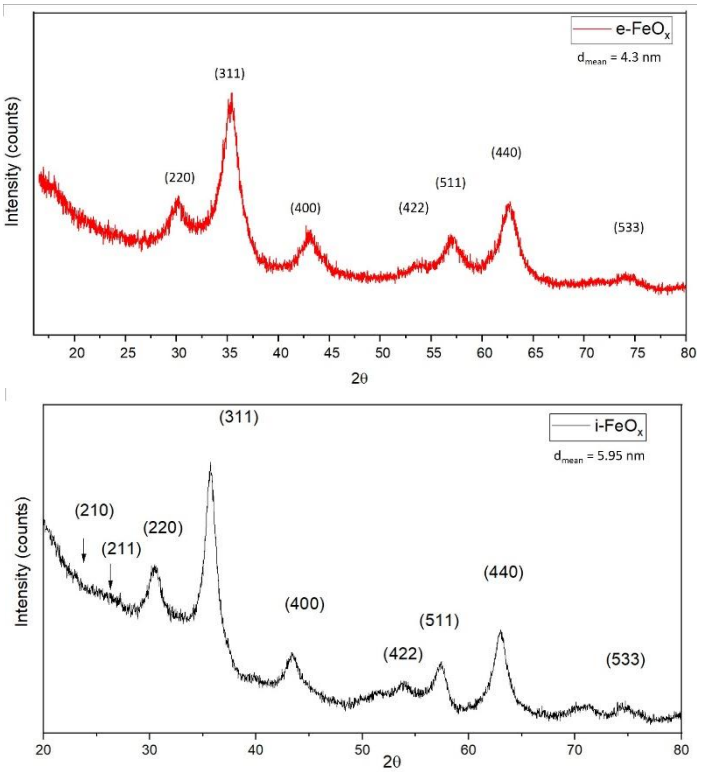

Fig. 3. X-ray diffractogram of e-FeO_x and i-FeO_x, respectively

The displayed patterns can be attributed to the cubic structure of the maghemite/magnetite phase (Fe_3O_4/γ-Fe_2O_3) corresponding to the JCPDS files 00-039-1346 and 00-019-0629. The mean diameter of the particles was calculated using Scherrer equation based on the linewidth of the (440) plane reflection peak and both samples present decreased particle sizes of under 6 nm. There are no noticeable differences between the two diffraction patterns, indicating that even though the sensitizer was different, the crystallographic nature of the samples remains the same.

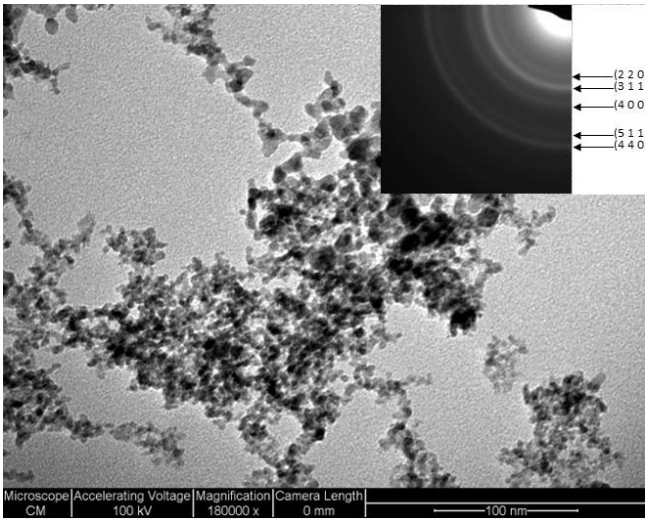

Fig. 4. TEM micrograph and SAED pattern in the insert of a reference sample

A reference sample was used for the morpho-structural characterization and the TEM micrograph can be observed in Fig. 4. It can be observed that the nanoparticles present a spherical morphology with a tendency to agglomerate into chain-like aggregates; morphological feature that has been previously displayed [16, 17]. In order to determine a mean nanoparticle size, image processing by ImageJ was attained and a dimension of 4.1 nm was calculated. Moreover, the ring pattern presented in the insert confirmed the results obtained by XRD analysis. Moreover, both samples exhibited excellent stability in water-based suspensions (Table 2).

The XPS survey spectra in Fig. 2(b) confirms the coexistence of C, O and Fe. By analysing the elemental composition evaluations determined by EDS (values mediated over the entire volume) and XPS (values specific for the surface layers; 0-2 nm) it can be observed that the C presence is considerably higher on the surface of the nanoparticles, being probably the result of a decomposition catalysed by the freshly nucleated iron cluster from the pyrolytic flame which leads to the decomposition of the organic components (ethene or isopropanol) from the precursor mix. Moreover, it can be noted that the C percentage is considerably

higher for the sample attained with ethene as a sensitizer (e-FeO_x – 30.1 at.%), than the one obtained with isopropanol as a sensitizer (i-FeO_x – 18.87 at.%). Therefore, it can be stated that the synthesis of iron oxide nanoparticles using isopropanol as sensitizer leads to substantially less C deposits on the nanoparticle surface than in the case of ethene, fact that also explains their enhanced dispersibility in water-based suspensions.

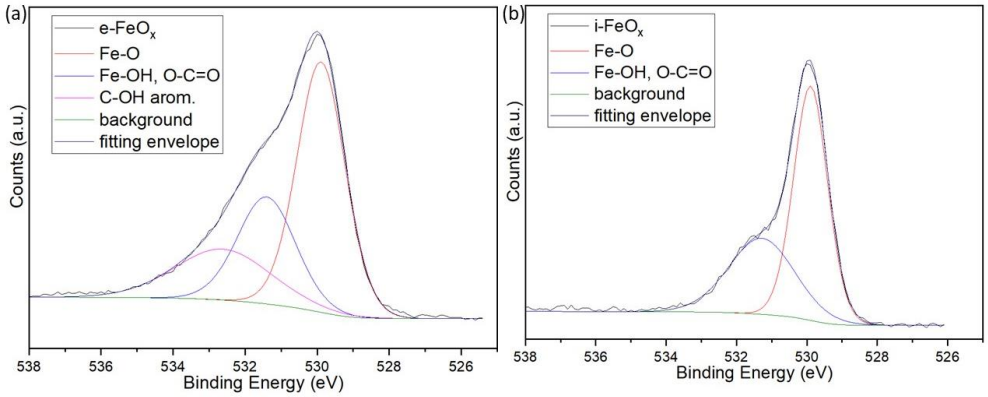

Fig. 5. XPS spectrum of high-resolution O 1s for (a) e-FeO_x and (b) i-FeO_x

The high-resolution XPS spectra for the O 1s active zone (binding energy – 525-540 eV) for e-FeO_x and i-FeO_x are presented in Fig. 5(a) and (b), respectively. These have been mathematically fitted with two or three peaks, using the Pseudo-Voight function. It can be observed that the primary peak (red, centred at 529.9 eV) has a value identical to the one that is considered to belong to the O^{2-} ion in the ionic bond with Fe^{3+} from Fe_2O_3, and different from Fe_3O_4 -529.7 eV) [17], the secondary peak (blue, centred at 531.4 eV) can be attributed to the Fe-OH bond [18], as well as to the functional groups O-C=O from the organic compounds [18, 19]. The presence of such functional groups (probably carboxylic type) may contribute to the surface acidity manifested by a reduced pH of the NPs-based water suspension from 5.8 from the used distilled water to 4.8 [20]. The third fitted peak in O 1s XPS spectrum (present only in the e-FeO_x sample, (a)), centred at 533.6 eV is usually ascribed to the C-OH aromatic bond. Comparing both O 1s spectra, the excellent fit of i-FeO_x O 1s curved with only two peaks can be emphasised (the first and second explained above), the contribution of C-OH groups is at least minimal for this sample and may explain the enhanced dispersibility in water-based suspensions.

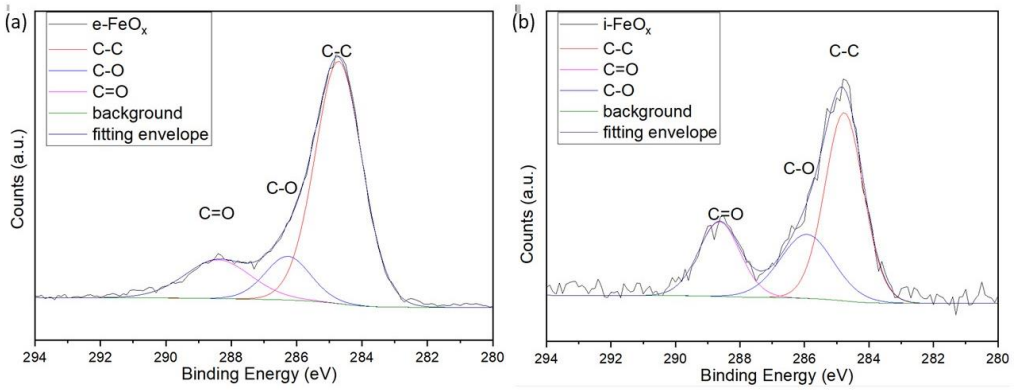

Fig. 6. XPS spectrum of high-resolution C 1s for (a) e-FeO_x and (b) i-FeO_x

The high-resolution C 1s spectrum (see Fig. 6) can be resolved into three fitted peaks centred at 284.7, 286.3, and 288.3 eV, belonging to C-C, C-O, and C=O, respectively [21]. Comparing both C 1s spectra, it can be clearly seen that the contribution from functional groups (C-O and C=O bonds) is much higher in the case of i-FeO_x, than e-FeO_x. Nevertheless, in both cases the majority of the C contribution comes from the C-C bond, probably as a carbonic sheet that partially covers the iron oxide nanoparticles; which are detrimental for the particle's disaggregation process.

3. Conclusions

The synthesis of iron oxide nanoparticles using laser pyrolysis and the influence of the sensitizer used has been investigated. Therefore, two separate laser pyrolysis experiments have been carried out with the use of two sensitizers (ethene and isopropanol). The morpho-structural characterization of the attained nanoparticles has been attained by XRD and TEM, both confirming the maghemite/magnetite phases, as well as the low dimensions of the particles. XRD patterns also revealed the preservation of the crystallographic nature of the sample, irrelevant of the sensitizer used. Moreover, the morphological pattern showed in the micrograph corresponded with previously obtained NPs, displaying spherical structures with a tendency to agglomerate in chain-like aggregates. Their stability, polydispersity index, and hydrodynamic dimension were determined using DLS with excellent results for both cases. Lastly, based on the XPS data obtained, it can be concluded that using isopropanol as a sensitizer considerably reduces the C content from the superficial layers of the nanoparticles.

Acknowledgements

This work was supported by the grant POCU/993/6/13 -153178, co-financed by the European Social Fund within the Sectorial Operational Program Human

Capital 2014 – 2020 and the Romanian Ministry of Research, Innovation and Digitalization under Romanian National Nucleu Program LAPLAS VII – contract no. 30N/2023.

R E F E R E N C E S

[1] I. Morjan et al., "Iron Oxide-Based Nanoparticles with Different Mean Sizes Obtained by the Laser Pyrolysis: Structural and Magnetic Properties," Journal of Nanoscience and Nanotechnology, **vol. 10,** no. 2, pp. 1223-1234, // 2010.

[2] T. Vangijzegem, D. Stanicki, and S. Laurent, "Magnetic iron oxide nanoparticles for drug delivery: applications and characteristics," Expert Opinion on Drug Delivery, **vol. 16**, no. 1, pp. 69-78, 2019/01/02 2019.

[3] R. Alexandrescu et al., "Reproducibility of the Synthesis of Iron Oxide Nanoparticles Produced by Laser Pyrolysis," AIP Conference Proceedings, **vol. 1275,** no. 1, pp. 30-32, 2010.

[4] S. Martelli et al., "Production of iron-oxide nanoparticles by laser-induced pyrolysis of gaseous precursors," Applied Surface Science, **vol. 154-155**, pp. 353-359, 2000/02/01/ 2000.

[5] A. V. Samrot, C. S. Sahithya, J. Selvarani A, S. K. Purayil, and P. Ponnaiah, "A review on synthesis, characterization and potential biological applications of superparamagnetic iron oxide nanoparticles," Current Research in Green and Sustainable Chemistry, **vol. 4**, p. 100042, 2021/01/01/ 2021.

[6] M. A. García et al., "Magnetic Properties of Fe Oxide Nanoparticles Produced by Laser Pyrolysis for Biomedical Applications," AIP Conference Proceedings, **vol. 1275**, no. 1, pp. 26-29, 2010.

[7] R. Alexandrescu et al., "Iron-oxide-based nanoparticles produced by pulsed infrared laser pyrolysis of Fe(CO)5," Materials Chemistry and Physics, **vol. 55**, no. 2, pp. 115-121, 1998/09/01/ 1998.

[8] F. Dumitrache et al., "Highly magnetic Fe2O3 nanoparticles synthesized by laser pyrolysis used for biological and heat transfer applications," Applied Surface Science, **vol. 336**, pp. 297-303, 2015/05/01/ 2015.

[9] H. Hofmeister et al., "Filamentary iron nanostructures from laser-induced pyrolysis of iron pentacarbonyl and ethylene mixtures," Applied Physics A, **vol. 72**, no. 1, pp. 7-11, 2001/01/01 2001.

[10] R. Alexandrescu et al., "Combining resonant/non-resonant processes: Nanometer-scale iron-based material preparation via CO2 laser pyrolysis," Applied Surface Science, **vol. 248,** no. 1, pp. 138-146, 2005/07/30/ 2005.

[11] S. Veintemillas-Verdaguer, M. P. Morales, and C. J. Serna, "Continuous production of γ-Fe2O3 ultrafine powders by laser pyrolysis," Materials Letters, **vol. 35**, no. 3, pp. 227-231, 1998/05/01/ 1998.

[12] R. Alexandrescu et al., "Photochemistry Aspects of the Laser Pyrolysis Addressing the Preparation of Oxide Semiconductor Photocatalysts," International Journal of Photoenergy, **vol. 2008**, p. 604181, 2008/08/20 2008.

[13] B. D. Green and J. I. Steinfeld, "Absorption coefficients for fourteen gases at CO2 laser frequencies," Applied Optics, **vol. 15**, no. 7, pp. 1688-1690, 1976/07/01 1976.

[14] G. Herzberg and B. L. Crawford, Jr., "Infrared and Raman Spectra of Polyatomic Molecules," The Journal of Physical Chemistry, **vol. 50**, no. 3, pp. 288-288, 1946/03/01 1946.

[15] A. A. E. Minea, "Advances in New Heat Transfer Fluids: From Numerical to Experimental Techniques (1st ed.)." CRC Press. https://doi.org/10.1201/9781315368184, 2017.

[16] I. I. Lungu et al., "Doxorubicin-Conjugated Iron Oxide Nanoparticles Synthesized by Laser Pyrolysis: In Vitro Study on Human Breast Cancer Cells," Polymers, **vol. 12**, no. 12. doi: 10.3390/polym12122799

[17] S. Nistorescu et al., "Low Blue Dose Photodynamic Therapy with Porphyrin-Iron Oxide Nanoparticles Complexes: In Vitro Study on Human Melanoma Cells," (in eng), Pharmaceutics, **vol. 13**, no. 12, Dec 10 2021.

[18] P. Chagas et al., "δ-FeOOH: a superparamagnetic material for controlled heat release under AC magnetic field," Journal of Nanoparticle Research, **vol. 15,** no. 4, p. 1544, 2013/03/03 2013.

[19] G. B. Beamson, D., "High Resolution XPS of Organic Polymers: The Scienta ESCA300 Database (Beamson, G.; Briggs, D.)," Journal of Chemical Education, **vol. 70**, no. 1, p. A25, 1993/01/01 1993.

[20] D. Hulicova-Jurcakova, M. Seredych, G. Q. Lu, and T. J. Bandosz, "Combined Effect of Nitrogen- and Oxygen-Containing Functional Groups of Microporous Activated Carbon on its Electrochemical Performance in Supercapacitors," Advanced Functional Materials, https://doi.org/10.1002/adfm.200801236 **vol. 19,** no. 3, pp. 438-447, 2009/02/10 2009.

[21] L. Qie et al., "Synthesis of functionalized 3D hierarchical porous carbon for high-performance supercapacitors,"Energy & Environmental Science, 10.1039/C3EE41638K **vol. 6**, no. 8, pp. 2497-2504, 2013.